Pergamon

PII: S0191-8141(96)00098-3

Journal of Structural Geology, Vol. 19, Nos 3–4, pp. 463 to 480, 1997

0191-8141/97 $17.00 + 0.00

Three-dimensional geometry and evolution of a segmented detachment fold, Mississippi Fan foldbelt, Gulf of Mexico

MARK G. ROWAN

Energy and Minerals Applied Research Center and Dept. of Geological Sciences, Campus Box 250, University of Colorado, Boulder, CO 80309, U.S.A.

(*Received* 1 *February* 1996; *accepted in revised form* 19 *September* 1996)

Abstract—The frontal fold of the deep-water Mississippi Fan foldbelt is used to investigate the relationships between folding and faulting in detachment folds. Seismic coverage shows the entire three-dimensional geometry, from termination to termination, and the deformation history as recorded by asymmetric growth strata on fold limbs. The fold is a salt-cored detachment fold cut by reverse faults on both limbs. Its three-dimensional geometry is complex, consisting of four separate culminations, each associated with a distinct fault or fault segment. Consequently, profile geometries vary significantly, but unsystematically, along strike.

Data analysis and structural restoration suggest a three-stage evolution during Mio-Pliocene shortening: (1) pre-existing, en-échelon salt pillows served as buckling instabilities for the initiation of detachment folds that experienced relatively minor lateral propagation during growth and linkage; (2) an increase in shortening rate was accommodated by break-thrust folding; and (3) the faults became inactive upon a decrease in shortening rate, such that further fold amplification occurred by rotation and uplift of the backlimb. There is a direct correlation between fold and fault geometries, and abundant evidence indicates that the geometries of individual fold segments dictated fault geometries.

INTRODUCTION

Many contractional folds are associated with faults that ramp up through strata. Three contrasting kinematic models can be differentiated on the basis of the relative timing of fault and fold initiation. Fault-bend folds (Suppe, 1983) form passively over pre-existing thrust faults with ramp-flat trajectories. In fault-propagation folds (Suppe, 1985; Jamison, 1987; Suppe and Medwedeff, 1990; Mitra, 1990), folding and faulting are synchronous, with folds growing as faults progressively cut up-section. In break-thrust folds (Willis, 1893; Fischer *et al.*, 1992), initially unfaulted detachment folds (De Sitter, 1956; Jamison, 1987; Dahlstrom, 1990; Poblet and McClay, 1996) are modified by reverse faults cutting fold limbs. Combinations of these fold types are also possible; for example, either fault-propagation or break-thrust folds can evolve into fault-bend folds if thrusts flatten into higher detachments.

In practice, it is difficult to deduce kinematics uniquely from the geometries of pretectonic layers, and recent studies have suggested that the geometry of growth strata preserved on fold limbs can be used to distinguish between the various kinematic models. Fault-bend folds are characterized by constant-thickness, rotated strata on backlimbs and growth strata that either thin over or onlap forelimbs (Medwedeff, 1989; Mount *et al.*, 1990; Suppe *et al.*, 1992; Hardy and Poblet, 1995; Hardy *et al.*, 1996). In fault-propagation folds, both backlimbs and forelimbs have complicated patterns of thinned, rotated, and onlapping growth sequences (Suppe *et al.*, 1992; Hardy and Poblet, 1995; Hardy *et al.*, 1996) that depend, in part, on the ramp angle (Ratliff, 1996, pers. comm.). Simple detachment folds may have progressively rotated growth strata that thin onto both limbs (Hardy and Poblet, 1994; Poblet and Hardy, 1995; Torrente and Kligfield, 1995; Hardy *et al.*, 1996) or complex patterns of rotated, constant-thickness beds and fanning growth wedges (Poblet *et al.*, 1997). To date, no growth models have been published for break-thrust folds.

Little treatment has been given to the three-dimensional geometry and kinematics of fault-related folding. Plane-strain fault-bend and fault-propagation fold models have been extended to three dimensions by modeling displacement variations along strike (Wilkerson *et al.*, 1991; Ratliff, 1992). The resulting geometries compare well with observed three-dimensional fold geometries (Medwedeff, 1989, 1992; Ratliff, 1992; Shaw *et al.*, 1994; Shaw and Suppe, 1994). Both experimental and field evidence show that detachment folds are periclinal, or doubly-plunging, in three dimensions (Dubey and Cobbold, 1977; Bamford and Ford, 1990; Rowan, 1993a), but any relationship to slip variation on underlying detachments is unknown. Finally, there are no systematic descriptions or models of the three-dimensional geometry and kinematics of break-thrust folds.

In this paper, I describe the three-dimensional geometry of one of the frontal folds within the Mississippi Fan foldbelt (MFFB), 280 km SSE of New Orleans in the northern Gulf of Mexico (Fig. 1). The fold is a salt-cored detachment fold cut by several high-angle reverse faults and with well-preserved growth sequences on both limbs. The three-dimensional geometry is complex, consisting of four separate culminations, each associated with a distinct fault or fault segment. I present evidence suggesting that: (a) each fold segment originated over a pre-existing salt pillow, (b) the various segments linked at

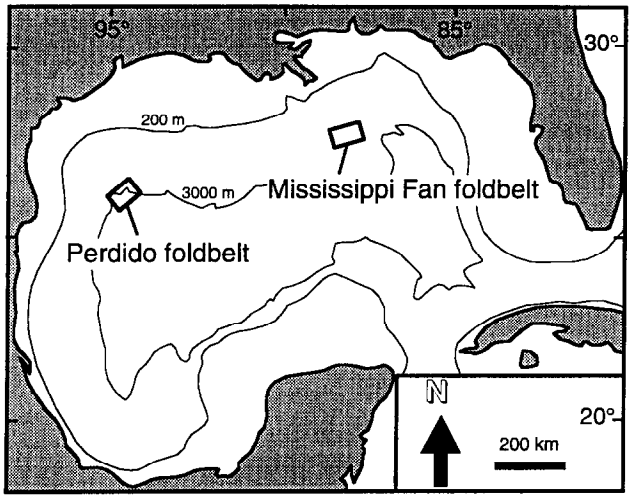

Fig. 1. Map of Gulf of Mexico showing location of the Missippi Fan and Perdido foldbelts. Water depth is contoured.

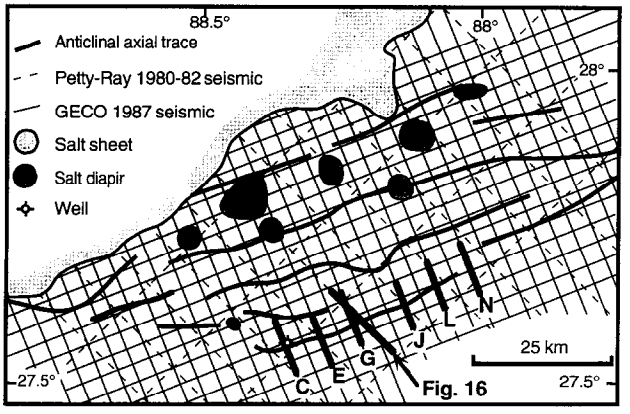

Fig. 2. Map of the Mississippi Fan foldbelt showing available seismic and well data. Structural features slightly modified from the interpretation of Weimer and Buffler (1992), which was based on old Halliburton seismic grid. C, E, G, J, L, and N are selected GECO-PRAKLA profiles across the frontal fold analyzed here and illustrated in Figs 4–10.

some stage with only minor subsequent lateral growth, (c) fault initiation was dictated by pre-existing fold geometries, and (d) there may be a positive correlation between the timing of faulting and increases in the regional shortening rate.

GEOLOGIC SETTING

The MFFB is one of several deep-water contractional belts located in the northern Gulf of Mexico. Both it and the Perdido foldbelt, located 600 km to the WSW (Fig. 1), formed at the basinward limit of the Jurassic Louann Salt in response to depositional loading and associated gravity spreading and/or sliding along a salt detachment linked to up-slope listric normal faults (Worrall and Snelson, 1989; Wu *et al.*, 1990a; Weimer and Buffler, 1992; Peel *et al.*, 1995; Diegel *et al.*, 1995; Trudgill *et al.*, 1995). Although salt has not been confirmed by well penetration within the MFFB, its presence is indicated by the presence along the folds of salt diapirs rising from the detachment level and by clearly imaged salt structures at the same stratigraphic level in unfolded regions to the east and northeast (Wu *et al.*, 1990a; DeBalko and Buffler, 1992; MacRae and Watkins, 1992; Weimer and Buffler, 1992).

The MFFB is characterized by ENE-trending anticlines and associated thrust faults (Fig. 2). Folds and faults are dominantly south-vergent, although symmetric box folds and backthrusts also exist (Weimer and Buffler, 1992). Only part of the MFFB can be observed because shallow allochthonous salt sheets of the Sigsbee Nappe have over-ridden and masked the seismic expression of the landward portions of the foldbelt (Fig. 2).

Folds within both the Mississippi Fan and Perdido foldbelts have been interpreted as salt-cored detachment folds (Worrall and Snelson, 1989; Wu *et al.*, 1990a; Weimer and Buffler, 1992; Rowan *et al.*, 1993; Diegel *et al.*, 1995; Peel *et al.*, 1995; Trudgill *et al.*, 1995). This contrasts with the interpretation of Mount *et al.* (1990), in which one of the Perdido folds was modeled as a fault-bend fold, cored by an imbricate horse, on the basis of the geometry of growth strata. Peel *et al.* (1995) and Trudgill *et al.* (1995) argued that this latter interpretation is incompatible with the observed fold geometries and regional considerations, and Rowan *et al.* (1993) showed that similar growth geometries can develop during break-thrust folding.

DATABASE AND METHODOLOGY

The primary seismic survey used in the interpretation was a 3×3 km grid of 56-fold, time-migrated data acquired and processed by GECO-PRAKLA in 1987 (Fig. 2). The processing sequence included predictive deconvolution, dip moveout (DMO) correction, velocity analysis every 2 km, and wave equation migration. A secondary survey used in some areas to tie lines was a 6×12 km grid of 24- and 48-fold data acquired by Petty-Ray (now Western Geophysical) from 1980 to 1983 (Fig. 2). The processing sequence for these data included spiking deconvolution, normal moveout correction, velocity analysis every 5 km, and FK (frequency) migration.

Limitations in data acquisition and artifacts generated during processing can create a variety of problems that may interfere with interpretation. First, the data may be under- or over-migrated such that reflections are positioned incorrectly on the profile. Concave-upward migration 'smiles' deep in the section are an example of over-migration. Second, faults or other velocity discontinuities may produce diffractions; an example can be seen near the tip of the back-thrust on Profile C (see Fig. 4). Third, multiples may be produced by seismic waves bouncing off the sea floor or other prominent boundaries. Fourth,

there may be sideswipe, where out-of-the-plane (three-dimensional) energy gets positioned on the 2-D profile. A probable example is the north-dipping event below the forelimb of Profile L (see Fig. 8), which may represent an adjacent thrust. Fifth, steep dips often cannot be imaged because seismic waves are reflected away from the receivers. Finally, areas of abundant fracturing and faulting are usually poorly imaged because of complex wave paths and energy dispersion. This can often be seen in the fold crest, where poor data were interpreted to result from numerous small-scale normal faults developed in response to outer-arc bending and extension during folding (see Figs 4–7).

Most of these artifacts and limitations can be recognized by an experienced interpreter. In some cases, they dictate that the data be ignored. For example, the strike line running along the steeply-dipping forelimb generally did not tie the dip lines because out-of-the-plane energy was incorrectly positioned. In other cases, artifacts can be used to guide the interpretation. For example, diffractions helped identify the presence and locations of faults. Ultimately, the dense and regular grid of data allowed for a well-constrained, internally consistent interpretation. Most importantly, forelimbs could be correlated accurately to backlimbs by tying around fault and fold terminations, thereby avoiding the uncertainties of cross-fault correlation and the problems of crestal erosion.

Two aspects of the interpretation merit further explanation. First, fault and horizon geometries were not interpreted below salt because of the poor data quality and the unknown amount of velocity pullup. These parts of the interpretations were added after depth conversion by extrapolation of clearly imaged geometries (compare Figs 4–9 with Fig. 10). Second, the interpretation of the frontal fault was problematic in some cases because of poor data quality (e.g. Figs 4 & 6). These zones of poor data could also be interpreted as a steep or overturned forelimb. However, the geometries of other profiles, where the zone is narrower or absent (e.g. Fig. 5 and especially Fig. 7), are more compatible with a fault interpretation. Even so, the exact location and geometry of the fault and the attitudes of bedding in the immediate hanging and footwalls could not be determined accurately. A best estimate was made for the fault location, and hanging and footwall horizons were simply extended through the zone of poor data to intersect the fault.

The Shell Atwater Valley 471-1, the only well in this portion of the foldbelt, penetrated the frontal fold analyzed in this study (Fig. 2) and provided age control for the interpretation. The well drilled the Pleistocene to upper Pliocene Mississippi Fan, through an unconformity at the fold crest into the middle Miocene, and finished in upper Oligocene strata (Figs 3 & 4). A synthetic seismogram was generated from the velocity log and tied to the seismic data; biostratigraphic data were then used to date the section between the unconformity and the bottom-hole depth. The Mississippi Fan

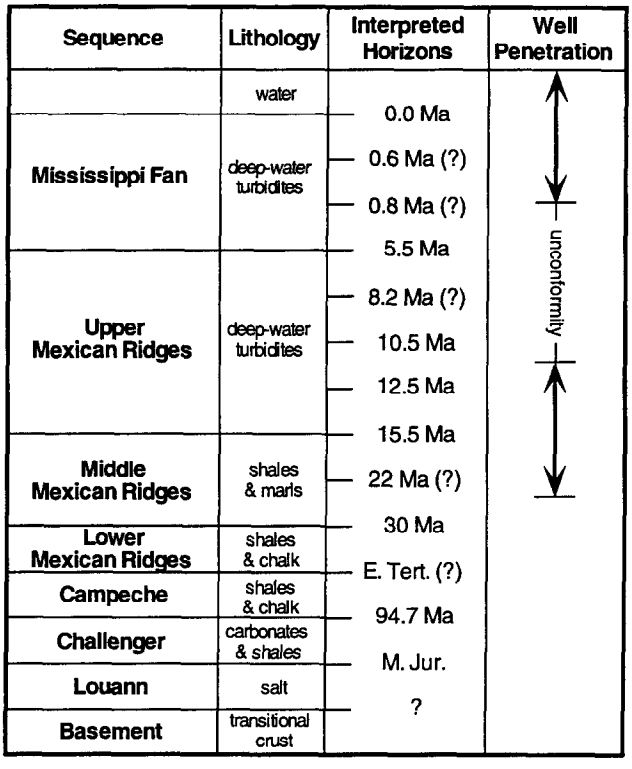

Fig. 3. Stratigraphic column showing sequence names, known or inferred lithologies, interpreted seismic horizons with ages, and the section penetrated by the Shell Atwater Valley 471-1 well. Compiled from Weimer (1990), Wu *et al.* (1990b), Feng and Buffler (1991), Weimer and Dixon (1994), and Feng (1995).

(above the unconformity), the eroded Plio-Miocene section, and the unpenetrated deeper strata (Fig. 3) were dated by correlation to regional seismic studies and regional well control (Weimer, 1990; Wu *et al.*, 1990b; Feng and Buffler, 1991; Weimer and Dixon, 1994; Feng, 1995). Although accurate age dates are not necessary for the geometric analysis presented here, they are critical when determining timing and rates of deformation.

The well data also provided velocity information for conversion of the time-migrated data to depth sections, but only at one point and over a limited time range. There are two end-member scenarios for lateral velocity variations and thus for depth conversion algorithms. First, velocity may simply be a function of depth below the water–sediment interface, in which case there are no lateral variations (except for where salt is involved, because of its constant velocity irrespective of depth). Alternatively, velocity may be a function of the stratigraphic layers (i.e. constant interval velocities), in which case there are significant variations from the fold to its flanks. The true velocity model almost certainly lies between these two extremes; lithology must play a role, but the depth of burial and attendant amount of compaction are also important factors.

Evidence regarding the true velocity distribution is equivocal. On the one hand, constant interval velocities are suggested by the approximately constant time thickness of some of the deeper units (the Lower Mexican

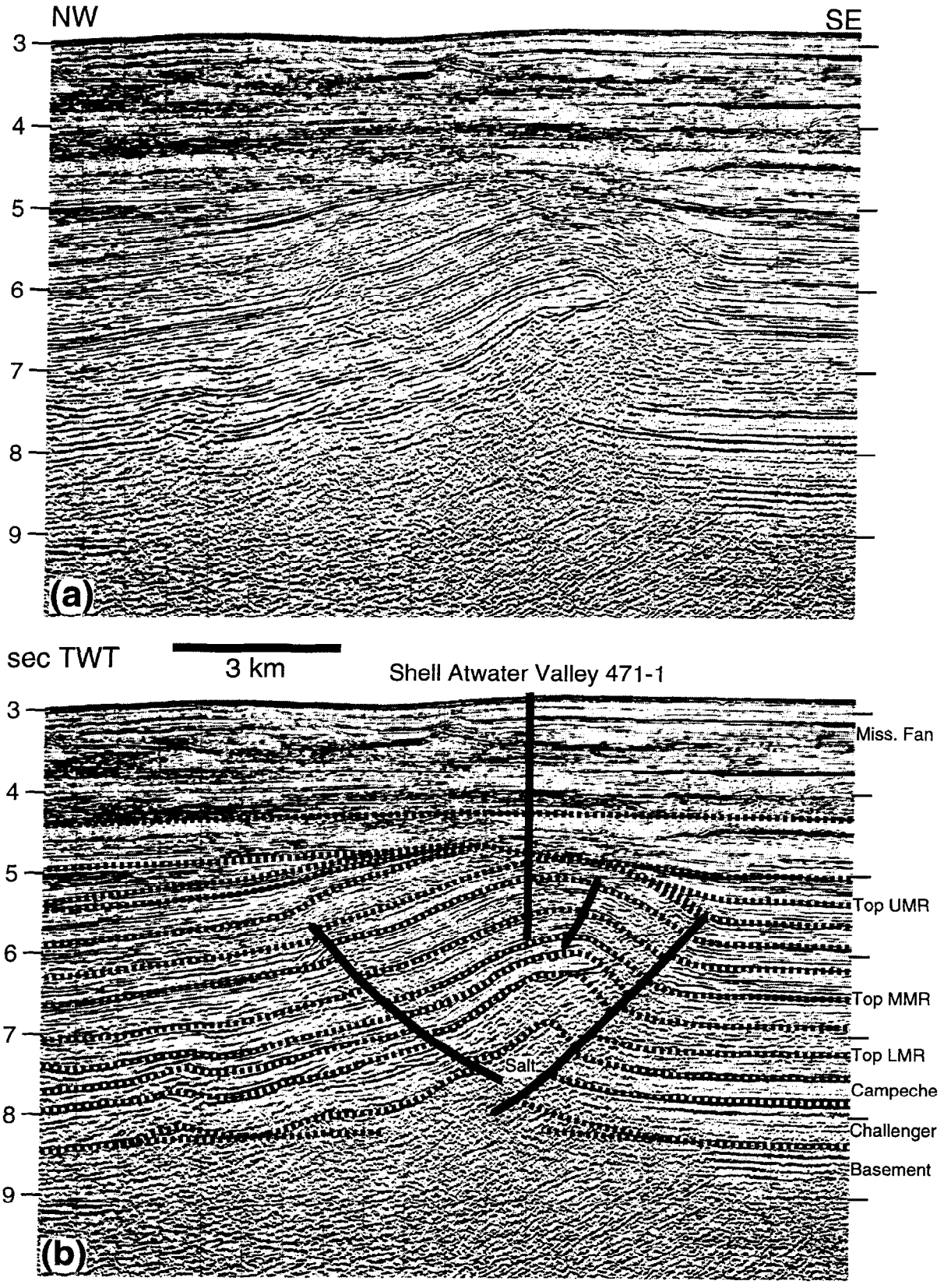

Fig. 4. Uninterpreted (a) and interpreted (b) versions of Profile C (located on Fig. 2). Vertical scale is in seconds of two-way travel time (TWT); profile is approximately 1:1. Data courtesy of GECO-PRAKLA.

Ridges [LMR] and lower Middle Mexican Ridges [MMR] units in Figs 4–9). On the other hand, there is little apparent velocity pull-up beneath the frontal fault where older rocks are juxtaposed against younger rocks (Figs 4–9). Although reflections do show curvature in this area, the geometry is more suggestive of real folding than velocity pull-up (the same curvature is seen where little or no fault offset exists in Figs 7 & 8). Therefore, depth conversion was conducted using a depth-dependent velocity function. One artifact of this simplification is that crestal portions of units are thinner in depth than is really the case, which becomes important in determing the onset of folding (see below).

The velocities of the deepest units are unknown. If the depth-dependent function determined from the well is projected to depth, relatively low velocities of about 3500 m s^{-1} are determined for the deepest units immediately above salt (presumed velocity of 4500 m s^{-1}). Yet there is little apparent velocity pull-up beneath interpreted salt (Figs 4–9), suggesting minimal velocity contrast. There are four possible explanations. First, velocities of deeper units may indeed be higher because they are thought to be carbonates. Second, the velocity of salt may be lower because of interlayering with carbonates and fine-grained clastics that might be expected at the depositional edge of the original salt basin (see below). Third, the salt cores may be small enough (in both area and thickness) that far offsets may correctly image the subsalt without any velocity artifacts. Finally, what is interpreted to be salt may in fact be shales. However, the presence of salt diapirs along the folds argues against this interpretation. The approach adopted in the depth conversions was to increase the velocities of the deepest units and slightly decrease that of salt to minimize the contrast and associated pull-up.

FOLD GEOMETRY

Profile geometry

Six selected seismic profiles, oriented approximately perpendicular to the fold axes, display two-dimensional geometries that vary markedly along strike from west to east: (a) Profile C (Fig. 4), near the well, shows an asymmetric fold with a major south-vergent reverse fault and a minor backthrust; (b) Profile E (Fig. 5) shows a more symmetrical fold, although the frontal fault is still larger than the backthrust; (c) the fold in Profile G (Fig. 6) is again asymmetrical, but with the long, planar backlimb not cut by a backthrust; (d) in Profile J (Fig. 7), the fold is tighter and more symmetrical, with smaller displacement on the frontal fault; (e) Profile L (Fig. 8) shows a perfectly symmetric detachment fold cut by a very small fault; and (f) Profile N (Fig. 9), at the eastern fold termination, displays a broad, low-relief detachment fold. Depth-converted interpretations are illustrated in Fig. 10.

The timing of deformation can be inferred from the interpreted stratal geometries. The shape of the salt core differs along strike, and thickness variations in the overlying Challenger and Campeche sequences suggest that some of this is due to early (Late Jurassic to Cretaceous) salt deformation. These thickness variations are not just artifacts of the depth conversion, because clear examples of thinning can be seen (e.g. on the backlimbs of Profiles C and G [Figs 4 & 6] and in the footwall of Profile J [Fig. 7]).

The onset of the main folding event is difficult to determine. The LMR and MMR units thin slightly over the fold crest (Fig. 10), but this could be an artifact of the depth conversion (i.e. using higher velocities in crestal areas could increase thicknesses there to show no variation). The only unequivocal evidence for thinning and thickening (i.e. onlap of reflections) in these intervals occurs in the upper MMR (e.g. crestal portion of Profile E [Fig. 5]); possible onlap is also interpreted in the lower MMR on the backlimb of Profile J (Fig. 7). In contrast, the upper part of the Campeche and the entire LMR show no evidence of onlap. Thus, the data suggest that there was a long period of tectonic quiescence from some time in the Late Cretaceous through the early Oligocene. Folding may have initiated during deposition of the MMR, between the late Oligocene and the early Miocene. Although there is no evidence of thickness variations across faults for these intervals, it is possible that faulting was also active.

Onlap onto anticlinal crests and cross-fault thickness changes within the lower Upper Mexican Ridges (UMR) show that folding and faulting were both definitely occurring during the middle to late Miocene (Figs 4–10). In contrast, the youngest growth strata, within the upper UMR and the lower Mississippi Fan (upper Miocene to Pliocene), are not faulted but display asymmetric growth patterns. Undeformed strata that simply onlap the forelimb and frontal fault are thinned, rotated, and uplifted on the backlimb. This pattern is observed even when the deeper fold is symmetric (Figs 8 & 10e). Finally, the main part of the Plio-Pleistocene Mississippi Fan is undeformed and erosionally truncates the highest portions of the fold (Figs 4, 6, & 10a, c).

Three-dimensional fault geometry

The profiles appear to show a systematic decrease in displacement on the frontal fault from west to east (Fig. 10). However, a map of the three-dimensional fault geometry shows that the frontal fault consists of three arcuate segments (Fig. 11). The western and central segments (I and II, respectively) are linked at a cusp in the vicinity of Profile E, whereas the eastern segment (III) is interpreted as a separate fault that overlaps the eastern tip of segment II (segment III could be linked to segment II, but the displacements on Profiles J and K are small enough that a relay zone is considered more likely). The backthrust is located in the vicinity of the cusp between

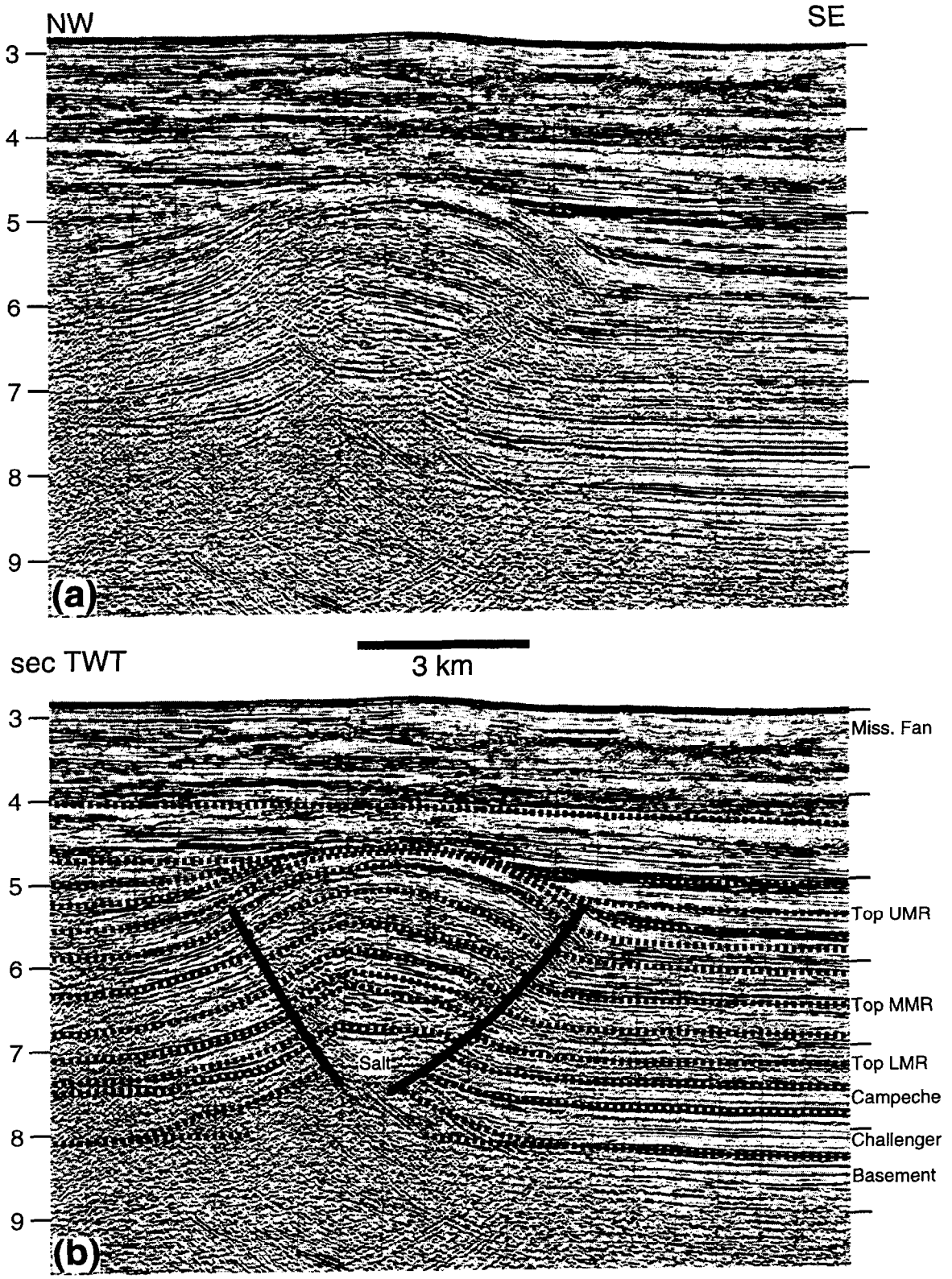

Fig. 5. Uninterpreted (a) and interpreted (b) versions of Profile E (located on Fig. 2). Vertical scale is in seconds of two-way travel time (TWT); profile is approximately 1:1. Data courtesy of GECO-PRAKLA.

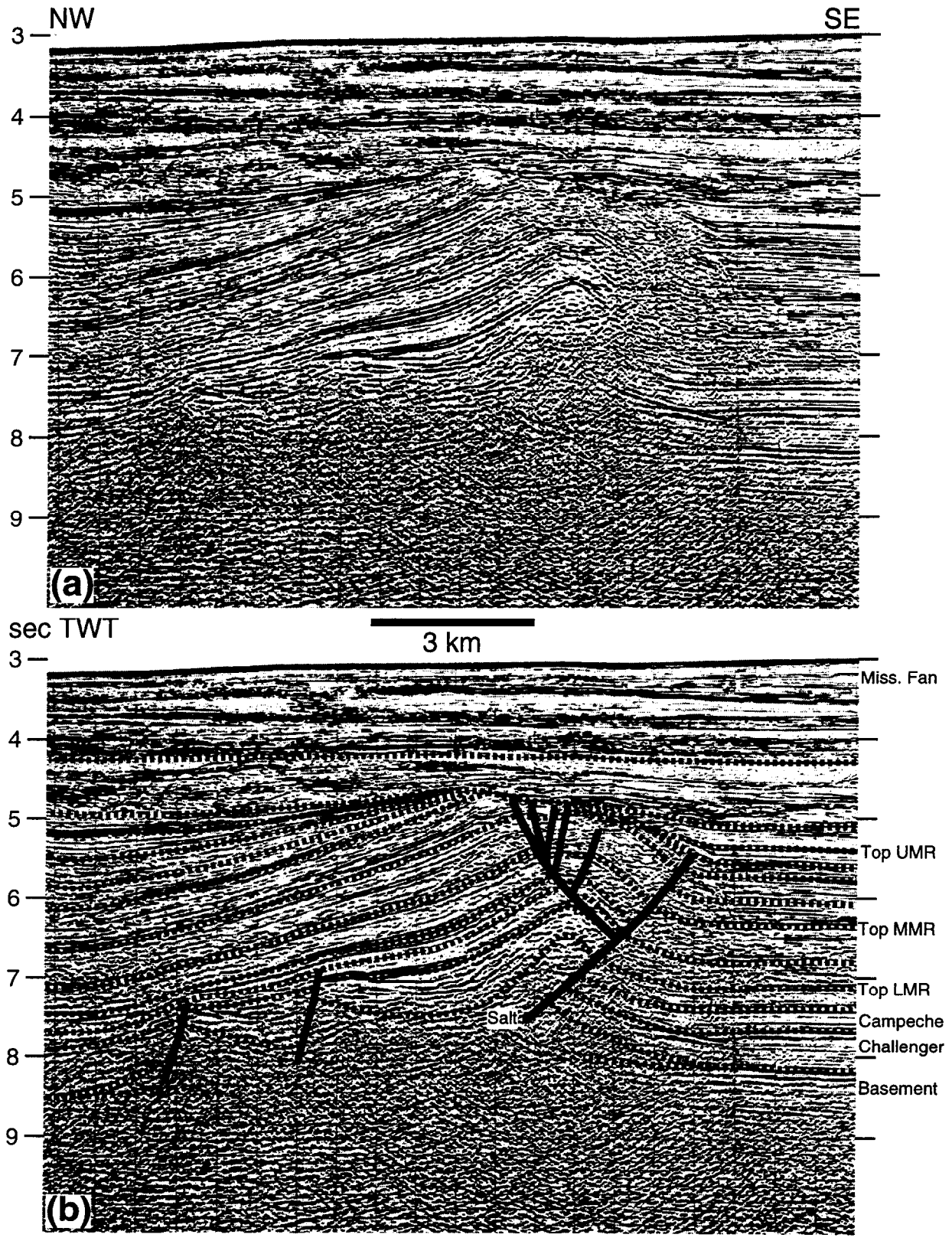

Fig. 6. Uninterpreted (a) and interpreted (b) versions of Profile E (located on Fig. 2). Vertical scale is in seconds of two-way travel time (TWT); profile is approximately 1:1. Data courtesy of GECO-PRAKLA.

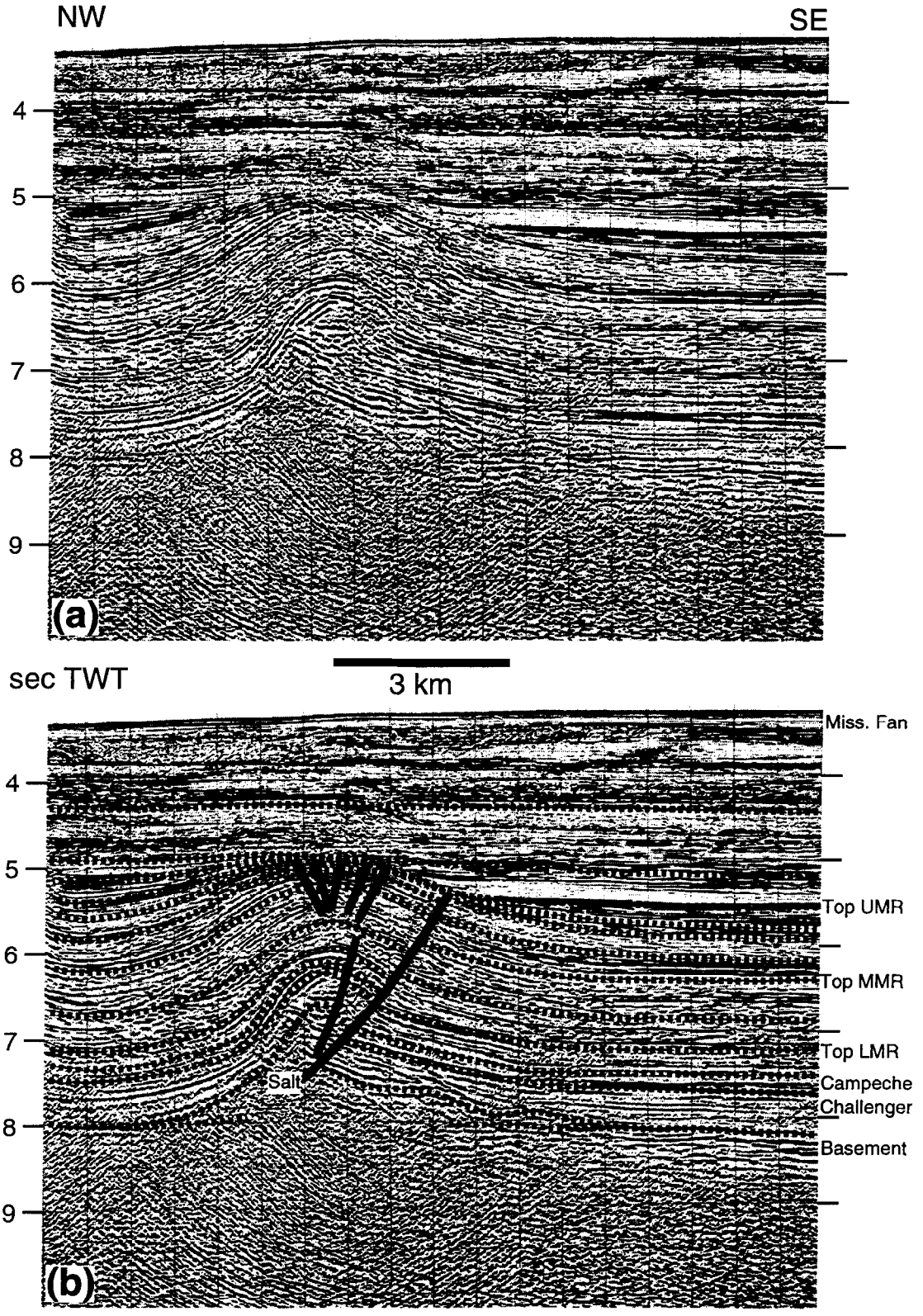

Fig. 7. Uninterpreted (a) and interpreted (b) versions of Profile J (located on Fig. 2). Vertical scale is in seconds of two-way travel time (TWT); profile is approximately 1:1. Data courtesy of GECO-PRAKLA.

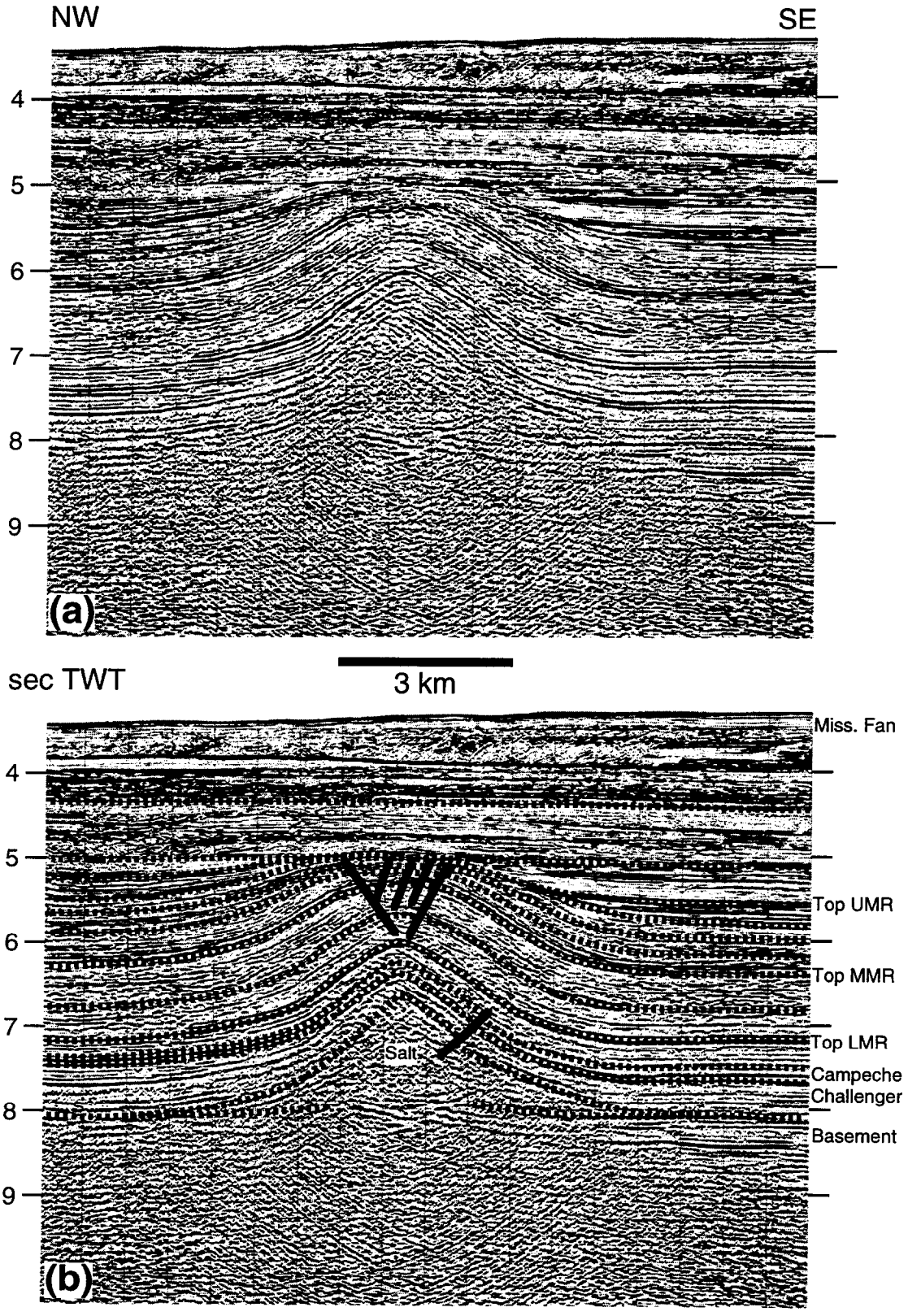

Fig. 8. Uninterpreted (a) and interpreted (b) versions of Profile L (located on Fig. 2). Vertical scale is in seconds of two-way travel time (TWT); profile is approximately 1:1. Data courtesy of GECO-PRAKLA.

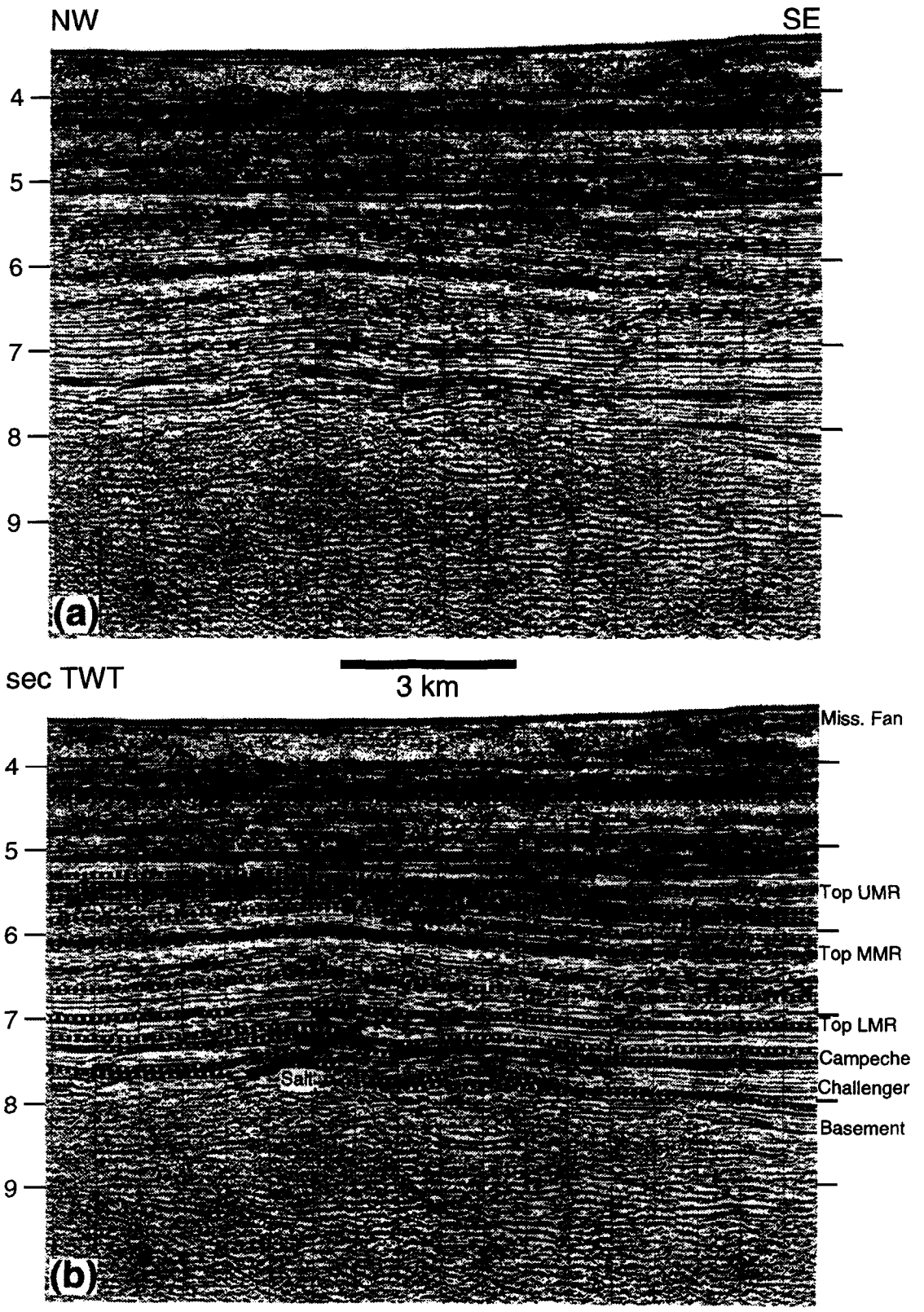

Fig. 9. Uninterpreted (a) and interpreted (b) versions of Profile N (located on Fig. 2). Vertical scale is in seconds of two-way travel time (TWT); profile is approximately 1:1. Data courtesy of GECO-PRAKLA.

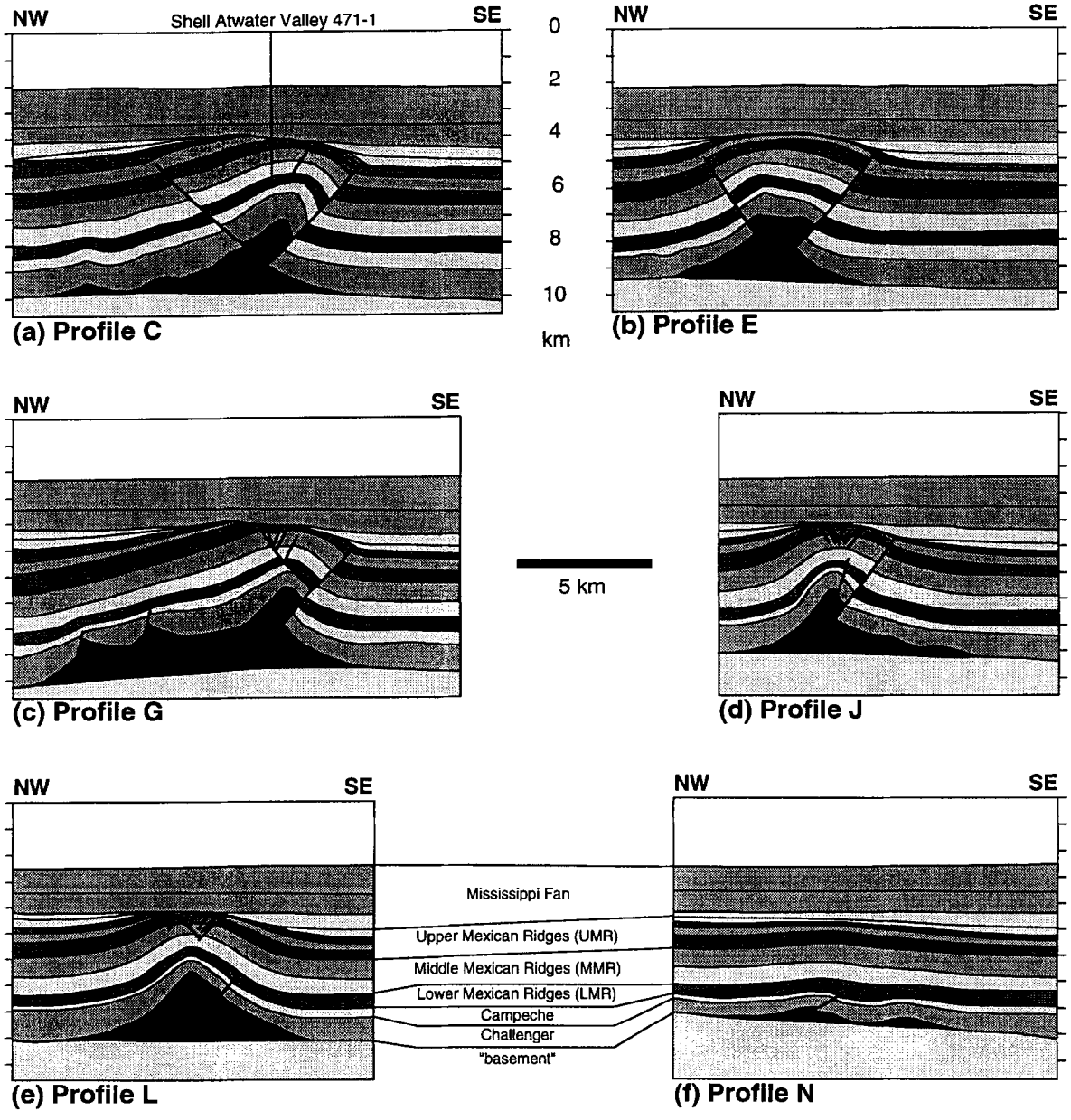

Fig. 10. 1:1 depth converted interpretations of the profiles illustrated in Figs 4–9. The interpretations here and in Figs 4–9 were derived from tying all dip and strike lines. Depth conversion carried out in GEOSEC using vertical ray paths and a depth-dependent velocity function derived from the Shell Atwater Valley 471-1 well (see text). Salt is black, water is white.

segments I and II. It may intersect the frontal fault along a branch line, as shown in Fig. 11, or the two faults may pass into zones of complex deformation within salt.

A plot of dip separation at the top of the Campeche illustrates the segmented nature of the frontal fault (Fig. 12). From west to east, there is an abnormally steep gradient (discussed below) from zero fault separation (no fault) on Profile A to a local maximum in dip separation at Profile B. Separation then decreases to a local minimum at Profile E (at the cusp), back to a local maximum at Profile F, and decreases to zero at Profile K, where the en-échelon overlap between segments II and III occurs. Segment III has much less separation, with a maximum at Profile M that decreases in both directions to zero at Profiles J and O.

Dip separation on the backthrust is a maximum at Profile E and decreases both west and east to zero at Profiles B and F. When the backthrust separation is added to that of frontal segments I and II, a smoother pattern is obtained (Fig. 12), showing that the backthrust accommodated the 'missing' displacement where segments I and II join. The curves plotted in Fig. 12 are similar to the patterns found in linked and overlapping normal faults (Peacock and Sanderson, 1991; Trudgill and Cartwright, 1994; Childs *et al.*, 1995).

The dip separation patterns should be considered as

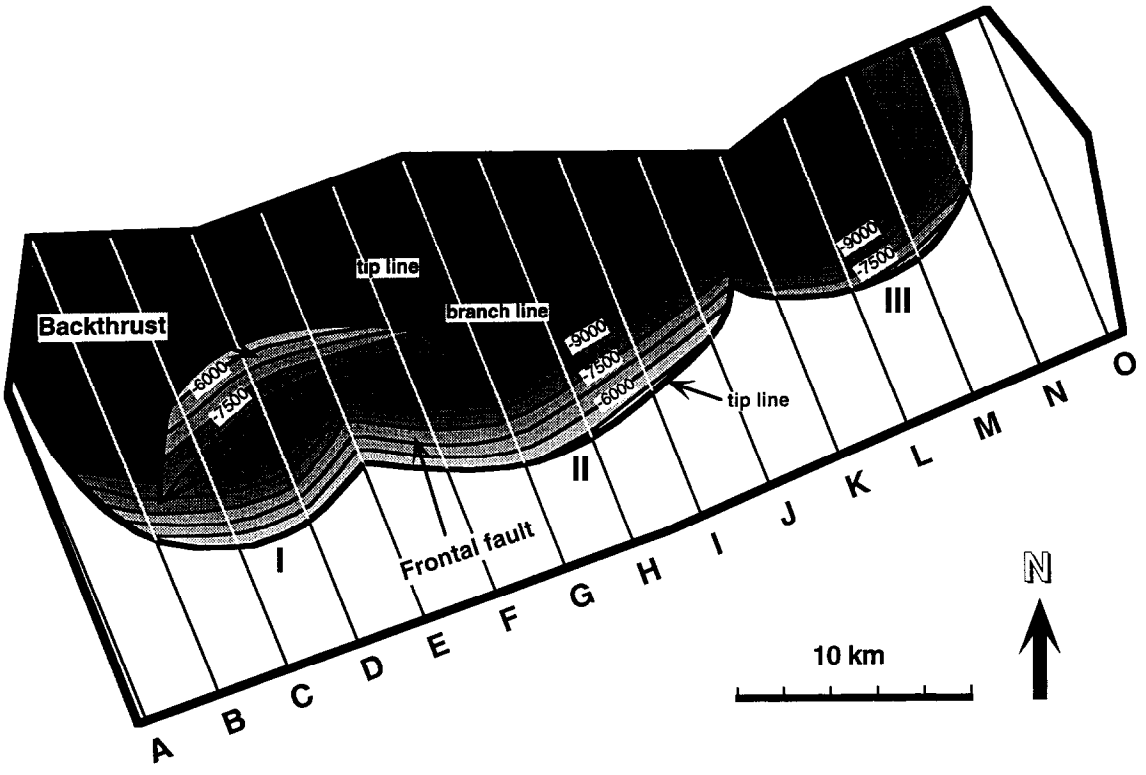

Fig. 11. Structure contour map of the linked fault system derived from a three-dimensional model constructed in GEOSEC-3D from the dip profiles. A–O are dip lines; I, II, and III are the three frontal fault segments: I and II are linked, II and III are interpreted to overlap. The backthrust and frontal fault may or may not intersect along a branch line. Darker shades are deeper, lighter shades are shallower (contour interval = 750 m).

approximations due to commonly poor data quality in the vicinity of the faults; separation values were derived by projecting well-imaged horizons into the zone of poor data. However, the reasonable correspondence between the mapped fault geometry, with its various segments (Fig. 11), and the separation patterns (Fig. 12) lends credence to the validity of the seismic interpretation.

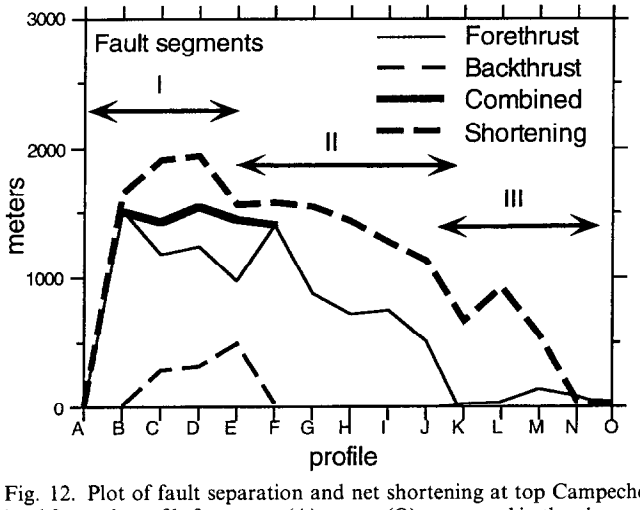

Fig. 12. Plot of fault separation and net shortening at top Campeche level for each profile from west (A) to east (O), measured in the plane of the profile. The frontal fault has three local maxima; the combined curve shows that the backthrust compensates for the minimum between segments I and II.

Three-dimensional fold geometry

The three-dimensional geometry of the fold is similarly segmented, with a separate culmination corresponding to each of the three frontal fault segments and the backthrust (Fig. 13). Fold segments I and II are separated by a saddle just northwest of the frontal fault cusp, whereas segments II and III overlap in an en-échelon pattern.

The variations in profile geometry illustrated in Fig. 10 can be related to their locations with respect to the segments and the local maxima/minima in fault separation (Fig. 13). Asymmetric fold geometries, with large-displacement frontal faults, characterize most of fold segments I and II (Profiles C and G, Figs 4, 6 & 10a, c). The saddles (minima) between segments I and II and between II and III have more symmetric, but still faulted, fold geometries (Profiles E and J, Figs 5, 7 & 10b, d). In contrast, fold segment III is typified by symmetric and largely unfaulted geometries (Profiles L and N, Figs 8, 9 & 10e, f).

DISCUSSION

Fold initiation

The presence of thickness variations in the Challenger and Campeche sequences, immediately above the salt,

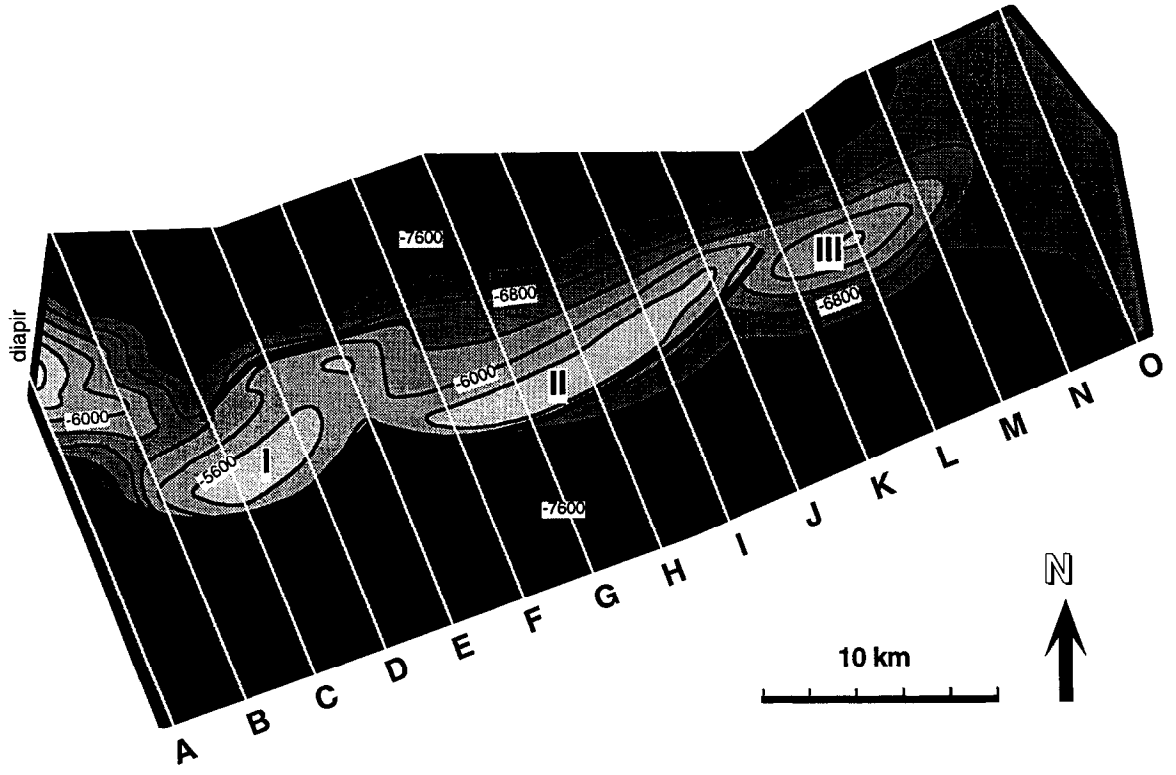

Fig. 13. Structure contour map of the top LMR (30 Ma) horizon derived from a three-dimensional model constructed in GEOSEC-3D from the dip profiles. Heavier lines are faults; A–O are dip lines; I, II, and III are the three fold segments. A salt diapir rooted in the detachment level is located just off the western end of the map. Lighter shades are highs, deeper shades are lows (contour interval = 400 m).

and the lack of such variations in the overlying LMR and lower MMR units, suggest that early salt structures existed prior to Tertiary shortening. An isopach map of the Challenger sequence shows a series of thinned areas that correspond to thick regions of salt which developed early. (Fig. 14). These are arranged in a right-stepping en-échelon pattern, and there is a strong positive correlation between the location and geometry of thin Challenger sequences and the major segments of the observed fold. Local onlap patterns show that this is not just an artifact of the interpretation, and the magnitude of the thinned regions is too large to be explained by errors in depth conversion. The implication is that old (Jurassic–Cretaceous) salt structures served as nucleation sites for later fold development during Miocene shortening.

The isopach map suggests that although old salt structures existed to the north of the fold, such structures were absent to the south (Fig. 14). Thus, the frontal edge of the fold probably represents the original basinward limit of salt (see also Fiduk *et al.*, 1995). The early salt structures may have been caused by differential sedimentary loading. Alternatively, their en-échelon pattern along the edge of salt (Fig. 14) suggests that they may have formed during an early phase of shortening that was oriented slightly oblique to the salt basin margin. The smaller wavelength of the early salt structures compared to that of the present folds (compare Figs 14 & 2) is compatible with initial buckling of a thinner multilayer. Early deformation may have been caused by minor gravity gliding above regionally south-dipping basement related to oceanic basin formation and associated subsidence during the Late Jurassic and Early Cretaceous. In contrast, Tertiary deformation was probably driven by gravity spreading, as sedimentary loading to the north caused a reversal of basement dip, which is currently to the north in this area (Sawyer *et al.*, 1991).

The dominant WSW trend of old salt structures changes abruptly at the southwestern termination of the fold to a NW–SE trend (Fig. 14). Again, this probably reflects the morphology of the original salt basin margin, with the NW–SE trend possibly related to transfer faults or accommodation zones within the rifted basement (Watkins *et al.*, 1995). This lateral boundary can explain the abrupt plunge at the western fold termination (Fig. 13) and the abnormally high displacement gradient on the frontal fault (Fig. 12).

Lateral fold growth and linkage

The lateral propagation of fault-related folds is commonly thought to be dependent on the lateral growth of the associated faults. Most models of fault growth are based on the expansion of an elliptical dislocation, with displacement related in various ways to fault dimension (Watterson, 1986; Walsh and Watter-

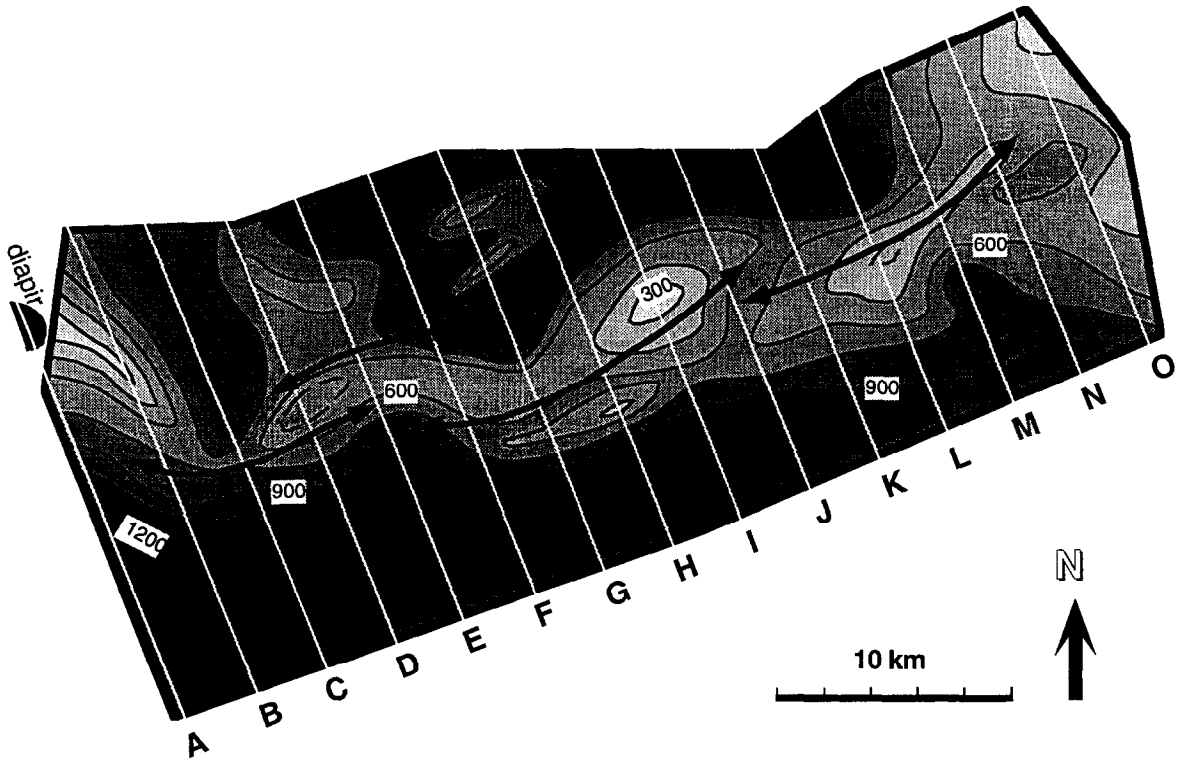

Fig. 14. Palinspastically restored isopach map of the Challenger sequence, derived from the dip profiles, showing the correspondence of early salt structures and the present fold geometry (crests shown by arrowed lines). A–O are dip lines. Thins (old salt highs) are shown by lighter shades, thicks (old salt lows) are in darker shades (contour interval = 150 m).

son, 1987; Marrett and Almendinger, 1991; Cowie and Scholz, 1992). Three-dimensional fault-bend and fault-propagation fold models, in turn, show lateral variations in geometry corresponding to lateral displacement gradients (Wilkerson *et al.*, 1991; Ratliff, 1992; Shaw *et al.*, 1994). The implication, either explicit or implicit, is that such folds initiate as small structures that propagate laterally through time. Likewise, experimental modeling shows that detachment folds initiate at small buckling instabilities and subsequently grow laterally with increased shortening (Dubey and Cobbold, 1977).

In contrast, the similarity between the geometry of the fold segments analyzed here (Fig. 13) and the size and shape of the early salt structures (Fig. 14) suggests that the Tertiary fold may have had an initial length close to that observed today. In essence, the early pillows would have served as large buckling instabilities. A relative lack of lateral growth is supported by an isopach map of one of the early growth intervals (Fig. 15). Thinned strata showing areas of active amplification from 15.5 to 12.5 Ma are of roughly the same size as the final fold segments, indicating only minor lateral propagation during the following 11 my of shortening and fold growth. One implication is that the various fold segments linked immediately or very early in the folding history.

Minimal lateral growth may be characteristic of salt-detached folds, in that the fold length is determined and limited by salt availability. It may also be that the fault scaling mentioned above is not applicable to salt; ductile shear is presumably not highly localized and progressive strain in salt probably has only minor effects on its rheology (Marrett, 1996, pers. comm.).

The relative lack of lateral growth had important implications for syntectonic sedimentation. Instead of the folds gradually growing in areal extent and only slowly choking off sediment transport pathways, the folds had an early impact on sea-floor topography. Sediments ponded north of the fold, possibly aided by local salt withdrawal as salt flowed into the fold core, and then spilled through the gap between fold segments I and II, over the frontal fault (which was active at the time), to form a local thickened region in the footwall between the two segments (Fig. 15).

Fold–fault relationships

I have demonstrated a clear geometric correlation between fault geometry and fold geometry. The relative timing of the two processes is not so easy to determine. Theoretically, faulting may have preceded folding (fault-bend folding), been coeval with folding (fault-propagation folding), or postdated folding (break-thrust folding). There are several lines of evidence that the latter history is the most appropriate kinematic model. First, the presence of a weak detachment layer and early salt pillows (Fig. 14) would have been mechanically favorable for the formation of detachment folds. Second, fold segment III, which accommodates less shortening than the other two

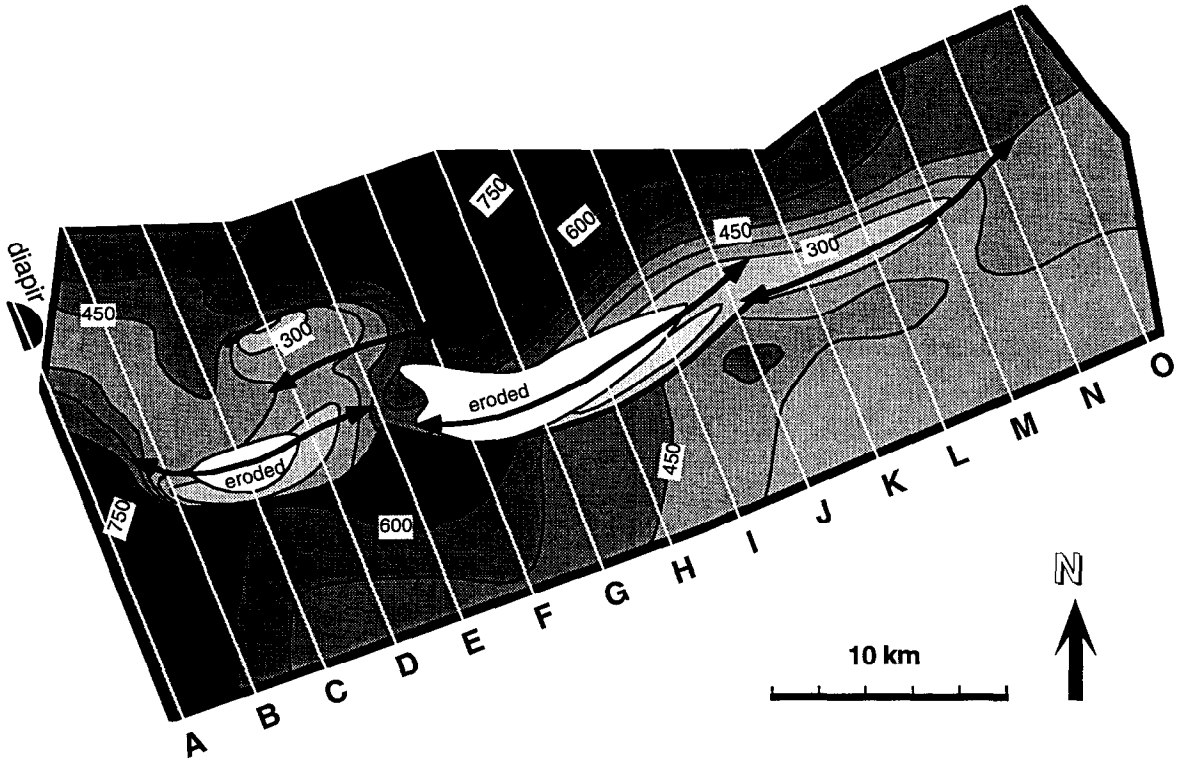

Fig. 15. Palinspastically restored isopach map of an early (15.5–12.5 Ma) growth interval, derived from the dip profiles. Areas of subsequent erosion are shown in white; arrowed lines are present-day fold crests; thick lines are faults; A–O are dip lines. Lighter shades show thins (areas of active uplift), darker shades show thicks (local depocenters) (contour interval = 75 m).

segments and thus may represent an immature example of the other folds, is primarily a detachment fold with only a minor fault (Figs 8, 9 & 10e, f). Third, there is no systematic relationship between fault displacement and total shortening: in segments I and II, faulting contributes a significant share of the net shortening, whereas shortening is accommodated almost entirely by folding in segment III (Fig. 12).

The observed geometries of growth strata may also be used to distinguish between the different fold models. The asymmetric pattern of rotated backlimb strata and unrotated, onlapping forelimb strata is similar to that predicted by fault-bend folding with either non-deposition or erosion at the fold crest (Suppe *et al.*, 1992, their fig. 13). However, backlimb growth strata in the MFFB do not have constant thickness, but instead thin onto the fold (Fig. 10), recording a progressive rotation of the backlimb that is incompatible with fault-bend folding over a fixed ramp. The growth geometry is somewhat similar to a detachment fold model in which both limbs lengthen and rotate, but in which the forelimb axial surface is pinned (Poblet *et al.*, 1997, their fig. 5b). Furthermore, the same asymmetric growth pattern is observed on segment III (Figs 8, 9 & 10e, f), which is an otherwise symmetric detachment fold and clearly not a fault-bend fold.

Restoration of a depth-converted profile (Fig. 16) documents, but does not prove, break-thrust kinematics (with a different interpretation and different assumptions, the profile could also be restored to support other kinematic models). Three stages of folding are proposed: (1) early detachment folding that initiated over pre-existing salt pillows (Fig. 16b); (2) break-thrust folding, with a fault cutting through the forelimb to the sea floor (Fig. 16c); and (3) late fold amplification, in which the fault was inactive and the backlimb was progressively rotated and uplifted (Fig. 16d).

The different stages illustrated in the restoration are representative of some of the observed strike-parallel variations in fold geometry: the detachment folding stage (Fig. 16b) is similar to the present geometry of segment III (Figs 8, 9 & 10e, f); the break-thrust phase, with a tighter fold (Fig. 16c), is analogous to profile geometries in the linkage/overlap zones between the different segments (Figs 5, 7 & 10b, d); and the fold amplification stage, with a long, more planar backlimb (Fig. 16d), is representative of the fold culminations (Figs 4, 7 & 10a, c). However, because of the inherited, segmented nature of the fold, there is no systematic relationship in which the geometric variations along strike are directly related to progressive stages in the evolutionary history.

The restorations suggest that activity on the thrust faults was confined to the middle stage of deformation. Cessation of thrusting can be clearly documented. First, the frontal fault is erosionally truncated at the same level within the UMR (the 10.5 Ma horizon) irrespective of the amount of displacement on the fault (Fig. 10). Second, overlying sequences simply onlap the forelimb but are

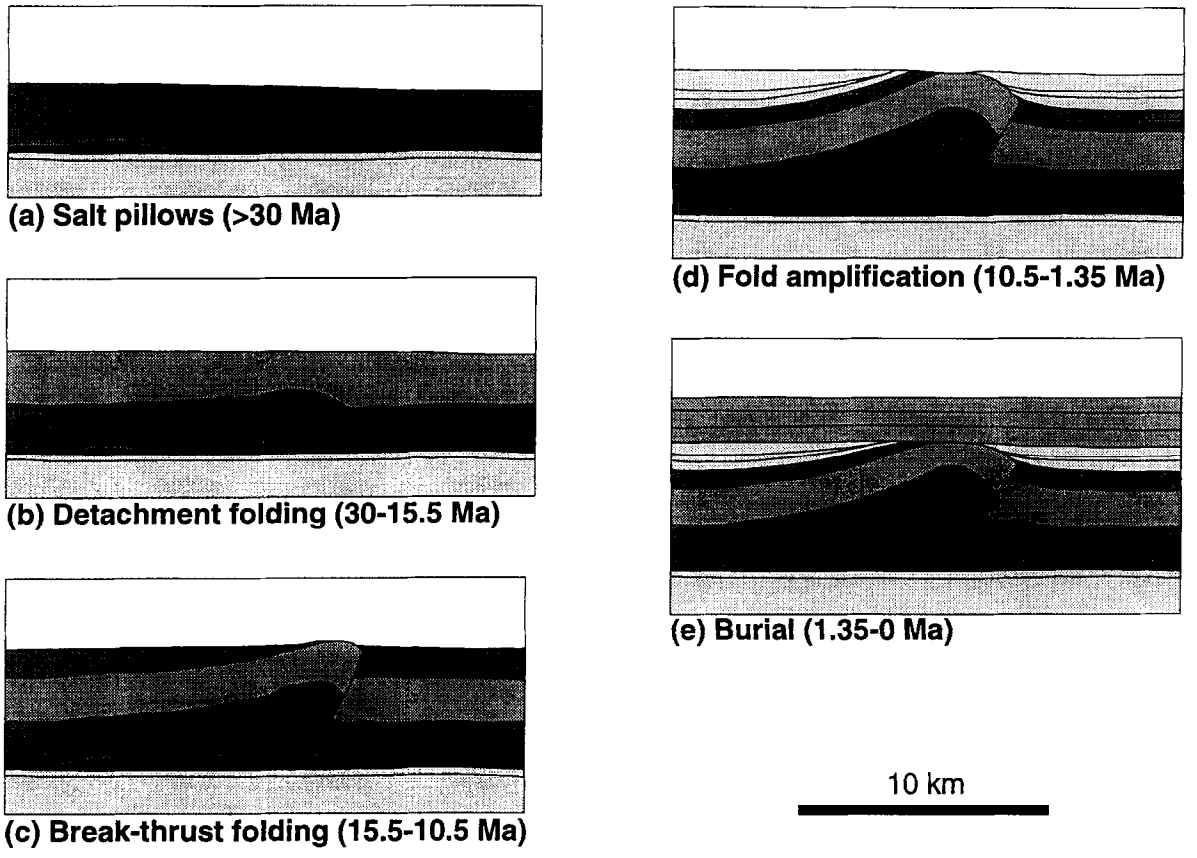

Fig. 16. Sequential restoration of depth-converted seismic profile (location shown in Fig. 2) showing different stages of structural evolution (adapted from Rowan *et al.*, 1993). Depth conversion used vertical ray paths and constant interval velocities. Restoration was carried out in GEOSEC: bed lenths were conserved for non-salt layers; salt was restored using the technique of Rowan (1993b), which places no constraints on salt area. The stratigraphy is slightly different from that shown in Figs 4–10 because it is from an earlier interpretation of the Petty-Ray (Western) data. Salt is black, water is white. No vertical exaggeration.

rotated and thinned on the backlimb, showing that fold growth continued after faulting ceased. Again, the resultant growth patterns are analogous to a detachment fold model with variable limb dip, variable limb length, and a fixed forelimb axial plane (Poblet *et al.*, 1997, their fig. 5b). In this model, the fold crest migrates towards the backlimb with time, which is compatible with the observation that thin strata in early growth intervals are located on present-day forelimbs (Fig. 15).

In contrast to the timing of fault cessation, the timing of thrust initiation cannot be determined. Although the restoration shows no fault in the early stages of deformation (Fig. 16b), this is not actually constrained by the restoration process, and it is possible that faulting was indeed active during this phase. An absence of early faulting, however, is supported by the presence of only minor thrusts in fold segment III. It is also compatible with changes in deformation rates measured from the restoration. The rate of shortening varied through time, with relatively slow rates prior to 15.5 Ma and after 10.5 Ma, and more rapid shortening between 15.5 and 10.5 Ma (Fig. 17). The slow rate after 10.5 Ma coincides with the period when the fault was inactive. It is possible that the earlier slow rate (prior to 15.5 Ma) also marks a time of folding without faulting, and that the higher rate corresponds to the break-thrust stage (Fig. 16c). In this scenario, faulting was a result of higher strain rates. Thus, after initial slow shortening formed detachment folds, more rapid gravity spreading was accommodated by a

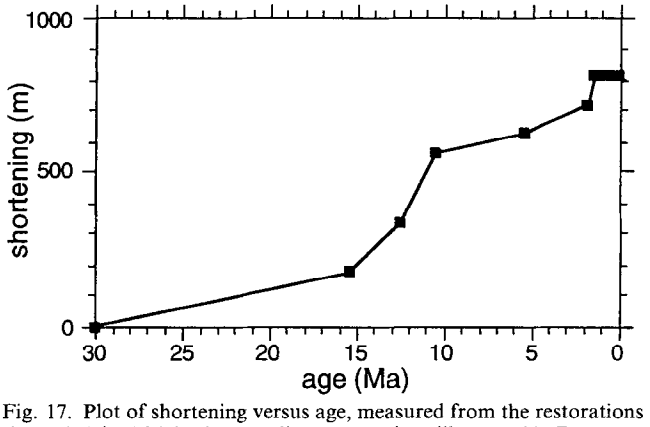

Fig. 17. Plot of shortening versus age, measured from the restorations shown in Fig. 16 (plus intermediate restorations illustrated in Rowan *et al.*, 1993). The period of more rapid shortening from 15.5 to 10.5 Ma corresponds to the break-thrust stage of deformation. The second pulse of rapid shortening (at about 2 Ma) may be an artifact of incorrect dating of horizons.

combination of folding and thrusting. Upon a subsequent decrease in the shortening rate, the faults became inactive and the folds amplified by backlimb rotation and uplift. The variations in shortening rate were presumably related to rates of depositional loading and extensional faulting up-dip to the north.

CONCLUSIONS

Folds within the Mississippi Fan foldbelt provide a natural laboratory for studying the three-dimensional geometry and evolution of contractional folds. Excellent three-dimensional seismic coverage over complete folds, from culminations to terminations, combined with a preserved record of growth strata on fold limbs, enable a thorough, four-dimensional analysis not possible in most other foldbelts. The major conclusions of this investigation of the frontal fold are listed below.

(1) The frontal fold of the Mississippi Fan foldbelt is a salt-cored, break-thrust fold. Its three-dimensional geometry is complex, consisting of four separate culminations, each corresponding to a distinct fault or fault segment. Profile geometries vary from symmetric detachment folds to asymmetric, faulted folds.

(2) The fold geometry was determined in large part by the location and shape of pre-existing salt pillows that formed during the Late Jurassic to Cretaceous. These served as buckling instabilities for later, Tertiary deformation. The fold appears to have initiated with an areal extent similar to that observed today; lateral propagation was probably minimal.

(3) Three stages of deformation are proposed: initial detachment folding from the late Oligocene to early Miocene; break-thrust folding in the middle Miocene; and fold amplification (without further faulting) from the late Miocene to Pliocene. Faulting appears to be have been caused by more rapid strain (shortening) rates.

(4) Break-thrust folds may contain asymmetric growth strata; in the studied fold, backlimb sequences are progressively thinned and rotated whereas forelimb strata are unfolded and simply onlap the fold. These patterns, although similar in some respects to those produced by fault-bend folds, are incompatible with translation over a fixed fault ramp.

(5) Although there is a clear and direct correlation between fold and fault geometries, there is abundant evidence that the fold segments dictated the fault geometries rather than vice versa. A similar relationship should be considered in analyses of other folds.

Acknowledgements—I wish to thank GECO-PRAKLA (especially Jerry Watson and David Risch) and Petty Ray (now Western Geophysical) for the seismic data, and CogniSeis Development for the GEOSEC and GEOSEC-3D restoration software. Funding was provided by the EMARC Gulf of Mexico industrial consortium at the University of Colorado (AGIP, Amoco, Anadarko, BHP, BP, Chevron, Conoco, CNG, Exxon, Marathon, Mobil, Pennzoil, Petrobras, Phillips, Shell, Texaco, Total, Union Pacific, and Unocal). T. Apotria, R. Marrett, B. Trudgill, C. Fiduk, P. Weimer, R. Ratliff, and R. Kligfield provided helpful discussion and/or comments on the manuscript.

REFERENCES

Bamford, M. and Ford, M. (1990) Flexural shear in a periclinal fold from the Irish Variscides. *Journal of Structural Geology* **12**, 59–67.

Childs, C., Watterson, J. and Walsh, J. J. (1995) Fault overlap zones within developing normal fault systems. *Journal of the Geological Society, London* **152**, 535–549.

Cowie, P. A. and Scholz, C. H. (1992) Growth of faults by accumulation of seismic slip. *Journal of Geophysical Research* **97**, 11,085–11,095.

Dahlstrom, C. D. A. (1990) Geometric constraints derived from the law of conservation of volume and applied to evolutionary models for detachment folding. *Bulletin of the American Association of Petroleum Geologists* **74**, 336–344.

DeBalko, D. A. and Buffler, R. T. (1992) Seismic stratigraphy and geologic history of Middle Jurassic through Lower Cretaceous rocks, deep eastern Gulf of Mexico. *Transactions of the Gulf Coast Association of Geological Societies* **42**, 89–105.

De Sitter, L. V. (1956) *Structural Geology*. McGraw-Hill, New York.

Diegel, F. A., Karlo, J. F., Schuster, D. C., Shoup, R. C., Tauvers, P. R. (1995) Cenozoic structural evolution and tectono-stratigraphic framework of the northern Gulf Coast continental margin. In *Salt Tectonics: A Global Perspective*, eds M. P. A. Jackson, D. G. Roberts and S. Snelson, Vol. 65, pp. 109–151.

Dubey, A. and Cobbold, P. (1977) Noncylindrical flexural slip folds in nature and experiments. *Tectonophysics* **38**, 223–239.

Feng, J. (1995) Post mid-Cretaceous seismic stratigraphy and geologic history, deep Gulf of Mexico basin. Unpublished Ph.D. thesis, University of Texas at Austin.

Feng, J. and Buffler, R. T. (1991) Preliminary age determinations for new deep Gulf of Mexico basin seismic sequences. *Gulf Coast Association of Geological Societies Proceedings*, 283–289.

Fiduk, J. C., McBride, B. C., Weimer, P., Rowan, M. G. and Trudgill, B. D. (1995) Defining the basinward limits of salt deposition, northern Gulf of Mexico. In *Salt, Sediment, and Hydrocarbons*, eds C. J. Travis, B. C. Vendeville, H. Harrison, F. J. Peel, H. R. Hudec and B. F. Perkins, pp. 53–64. Gulf Coast Section, SEPM Foundation Sixteenth Annual Research Conference, Program with Papers.

Fischer, M., Woodward, N. and Mitchell, M. (1992) The kinematics of break-thrust folds. *Journal of Structural Geology* **14**, 451–460.

Hardy, S. and Poblet, J. (1994) Geometric and numerical model of progressive limb rotation in detachment folds. *Geology* **22**, 371–374.

Hardy, S. and Poblet, J. (1995) The velocity description of deformation. Paper 2: sediment geometries associated with fault-bend and fault-propagation folds. *Marine and Petroleum Geology* **12**, 165–176.

Hardy, S., Poblet, J., McClay, K. and Waltham, D. (1996) Mathematical modelling of growth strata associated with fault-related fold structures. In *Modern Developments in Structural Interpretation, Validation and Modelling*, eds P. G. Buchanan and D. A. Nieuwland, Geological Society Special Publication, pp. 265–282, 99.

Jamison, J. (1987) Geometric analysis of fold development in overthrust terrains. *Journal of Structural Geology* **9**, 207–219.

MacRae, G. and Watkins, J. S. (1992) Evolution of the Destin Dome, offshore Florida, north-eastern Gulf of Mexico. *Marine and Petroleum Geology* **9**, 501–509.

Marrett, R. and Almendinger, R. (1991) Estimates of strain due to brittle faulting: sampling of fault populations. *Journal of Structural Geology* **13**, 735–738.

Medwedeff, D. (1989) Growth fault-bend folding at southeast Lost Hills, San Joaquin Valley California. *Bulletin of the American Association of Petroleum Geologists* **73**, 54–67.

Medwedeff, D. A. (1992) Geometry and kinematics of an active, laterally propagating wedge thrust, Wheeler Ridge, California. In *Structural Geology of Fold and Thrust Belts*, eds S. Mitra and G. W. Fisher, pp. 3–28. Johns Hopkins University Press, Baltimore.

Mitra, S. (1990) Fault-propagation folds: geometry, kinematic evolution, and hydrocarbon traps. *Bulletin of the American Association of Petroleum Geologists* **74**, 921–945.

Mount, V. S., Suppe, J. and Hook, S. (1990) A forward modeling strategy for balancing cross-sections. *Bulletin of the American Association of Petroleum Geologists* **74**, 521–531.

Peacock, D. C. P. and Sanderson, D. J. (1991) Displacements, segment

linkage and relay ramps in normal fault zones. *Journal of Structural Geology* **13**, 721–733.

Peel, F. J., Travis, C. J. and Hossack, J. R. (1995) Genetic structural provinces and salt tectonics of the Cenozoic offshore US Gulf of Mexico: a preliminary analysis. In *Salt Tectonics: A Global Perspective*, eds M. P. A. Jackson, D. G. Roberts and S. Snelson, Vol. 65, pp. 153–175. American Association of Petroleum Geologists Memoirs.

Poblet, J. and Hardy, S. (1995) Reverse modelling of detachment folds: application to the Pico del Aguila anticline in the South Central Pyrenees (Spain). *Journal of Structural Geology* **17**, 1707–1724.

Poblet, J. and McClay, K. (1996) Geometry and kinematics of single-layer detachment folds. *Bulletin of the American Association of Petroleum Geologists* **80**, 1085–1109.

Poblet, J., McClay, K., Storti, F. and Muñoz, J. A. (1997) Geometries of syntectonic sediments associated with single-layer detachment folds. *Journal of Structural Geology* **19**, 369–381.

Ratliff, R. (1992) Deformation studies of folding and faulting: cross-section kinematics, strain analysis, and three-dimensional geometry. Unpublished Ph.D. thesis, University of Colorado, Boulder.

Rowan, M. G. (1993a) Structural geometry of the Wildhorn Nappe between the Aar massif and the Brienzer See. *Eclogae Geologicae Helvetiae* **86**, 87–119.

Rowan, M. G. (1993b) A systematic technique for the sequential restoration of salt structures. *Tectonophysics* **228**, 331–348.

Rowan, M. G., Kligfield, R. and Weimer, P. (1993) Processes and rates of deformation: preliminary results from the Mississippi Fan fold-belt, deep Gulf of Mexico. In *Rates of Geologic Processes*, eds J. M. Armentrout, R. Bloch, H. C. Olson and B. F. Perkins, pp. 209–218. Gulf Coast Section, SEPM Foundation Fourteenth Annual Research Conference, Program with Papers.

Sawyer, D. S., Buffler, R. T. and Pilger, R. H. Jr (1991) The crust under the Gulf of Mexico basin. In *The Gulf of Mexico Basin*, ed. A. Salvador, Vol. J, pp. 53–72. Geological Society of America, The Geology of North America.

Shaw, J. H., Hook, S. C. and Suppe, J. (1994) Structural trend analysis by axial surface mapping. *Bulletin of the American Association of Petroleum Geologists* **78**, 700–721.

Shaw, J. H. and Suppe, J. (1994) Active faulting and growth folding in the eastern Santa Barbara Channel, California. *Bulletin of the Geological Society of America* **106**, 607–626.

Suppe, J. (1983) Geometry and kinematics of fault-bend folding. *American Journal of Science* **283**, 684–721.

Suppe, J. (1985) *Principles of Structural Geology*. Prentice-Hall, Inc., Englewood Cliffs, NJ.

Suppe, J. and Medwedeff, D. (1990) Geometry and kinematics of fault-propagation folding. *Eclogae Geologicae Helvetiae* **83**, 409–454.

Suppe, J., Chou, G. and Hook, S. (1992) Rates of folding and faulting determined from growth strata. In *Thrust Tectonics*, ed. K. McClay, pp. 105–122. Chapman and Hall, London.

Torrente, M. M. and Kligfield, R. (1995) Modellizzazione predittiva di pieghe sinsedimentarie. *Bulletin of the Geological Society, Italy* **114**, 293–309.

Trudgill, B. D. and Cartwright, J. A. (1994) Relay ramp forms and normal fault linkages—Canyonlands National Park, Utah. *Bulletin of the Geological Society of America* **106**, 1143–1157.

Trudgill, B. D., Rowan, M. G., Fiduk, J. C., Weimer, P., Gale, P. E., Korn, B. E., Phair, R. L., Gafford, W. T., Dischinger, J. B., Roberts, G. R. and Henage, L. F. (1995) The tectono-stratigraphic evolution of the salt-related Perdido foldbelt, Alaminos Canyon, northwestern deep Gulf of Mexico. In *Salt, Sediment, and Hydrocarbons*, eds C. J. Travis, B. C. Vendeville, H. Harrison, F. J. Peel, H. R. Hudec and B. F. Perkins, pp. 275–284. Gulf Coast Section, SEPM Foundation Sixteenth Annual Research Conference, Program with Papers.

Walsh, J. J. and Watterson, J. (1987) Distributions of cumulative displacement and seismic slip on a single normal fault surface. *Journal of Structural Geology* **9**, 1039–1046.

Watkins, J. S., MacRae, G. and Simmons, G. R. (1995) Bipolar simple-shear rifting responsible for distribution of mega-salt basins in Gulf of Mexico? In *Salt, Sediment, and Hydrocarbons*, eds C. J. Travis, B. C. Vendeville, H. Harrison, F. J. Peel, H. R. Hudec and B. F. Perkins, pp. 297–305. Gulf Coast Section, SEPM Foundation Sixteenth Annual Research Conference, Program with Papers.

Watterson, J. (1986) Fault dimensions, displacements and growth. *Pure and Applied Geophysics* **124**, 365–373.

Weimer, P. (1990) Sequence stratigraphy, facies geometries, and depositional history of the Mississippi Fan, deep Gulf of Mexico. *Bulletin of the American Association of Petroleum Geologists* **74**, 225–253.

Weimer, P. and Buffler, R. (1992) Structural geology and evolution of the Mississippi Fan Fold Belt, deep Gulf of Mexico. *Bulletin of the American Association of Petroleum Geologists* **76**, 225–251.

Weimer, P. and Dixon, B. T. (1994) Regional sequence stratigraphic setting of the Mississippi Fan complex (late Miocene to present), northern deep Gulf of Mexico: implications for the evolution of the northern Gulf Basin margin. In *Submarine Fans and Turbidite Systems: Sequence Stratigraphy, Reservoir Architecture, and Production Characteristics*, eds P. Weimer and A. H. Bouma, pp. 373–381. Gulf Coast Section, SEPM Foundation Fifteenth Annual Research Conference, Program with Papers.

Wilkerson, M., Medwedeff, D. and Marshak, S. (1991) Geometrical modeling of fault-related folds: a pseudo-three dimensional approach. *Journal of Structural Geology* **13**, 801–812.

Willis, B. (1893) *Mechanics of Appalachian Structure*. USGS Annual Report **13** (1891–1892), part 2, 217–281.

Worrall, D. M. and Snelson, S. (1989). Evolution of the northern Gulf of Mexico, with emphasis on Cenozoic growth faulting and the role of salt. In *The Geology of North America: an Overview*, eds A. W. Bally and A. R. Palmer, Vol. A, pp. 97–138. Geological Society of America. Decade of North American Geology.

Wu, S., Bally, A. W. and Cramez, C. (1990a) Allochthonous salt, structure and stratigraphy of the north-eastern Gulf of Mexico, part II: structure. *Marine and Petroleum Geology* **7**, 334–370.

Wu, S., Vail, P. R. and Cramez, C. (1990b) Allochthonous salt, structure and stratigraphy of the north-eastern Gulf of Mexico, part I: stratigraphy. *Marine and Petroleum Geology* **7**, 318–333.